Impacts of Laboratory Vibrations and Laser Flicker Noise on Digital Holography

Douglas E. Thornton[ID], Mark F. Spencer[ID], Christopher A. Rice[ID], and Glen P. Perram

Abstract— In this paper, we experimentally demonstrate the impacts of laboratory vibrations and laser flicker noise on digital holography (DH). Specifically, we measure both the vibration efficiency and the coherence efficiency of our DH system at various focal-plane array integration times and path-length differences between the signal and reference. These efficiencies, in practice, contribute to the overall mixing efficiency, which is a measure for how well the detected signal and reference interfere. The results show that when the integration time is ≤1 ms, the laboratory vibrations are negligible with a vibration efficiency of 100%; however, when the integration time equals 100 ms, the laboratory vibrations lead to a 94% vibration efficiency. In addition, the results show that the effective coherence length of the master-oscillator (MO) laser increases by 280% when the integration time decreases from 100 ms to 100 µs. To account for this outcome, we present a model of the coherence efficiency based on the frequency noise of the MO laser. The model fit to the DH data then shows that the frequency of the MO laser is flicker-noise dominated. As a result, decreasing the integration time improves the overall mixing efficiency because of high-pass filtering in both the vibration efficiency and the coherence efficiency. Based on previous published efforts, these results have direct ties to the achievable signal-to-noise ratio of a DH system.

Index Terms— Digital holography, noise, coherence.

I. Introduction

APPLICATIONS of digital holography (DH) are diverse with significantly different system requirements. For applications like microscopy, the path-length differences between the signal and reference are nearly matched and do not limit the achievable signal-to-noise ratio (SNR) due to the coherence length of the light source. In fact, these applications often use laser sources with a short coherence length [1], [2] or even incoherent light sources [3]. However, for applications like wavefront sensing [4]–[6] and long-range imaging [7]–[9], the coherence length of the master-oscillator (MO) laser is a range-limiting factor. For tactical applications, where the DH system is on a moving platform, external factors, such as vibrations, will also degrade performance. Therefore, understanding the effects of coherence and vibrations in terms

of the achievable SNR of a DH system is critical for these larger-scale applications.

Since the achievable SNR of a DH system depends on many factors, it is convenient to treat each performance-limiting effect as a multiplicative loss or "efficiency" in the derived SNR expression. Moving forward we need to measure these efficiencies in order to characterize the performance of a fielded DH system. The mixing efficiency, in practice, is a measure for how well the detected signal and reference interfere. Thus, it consists of multiple efficiencies from independent sources and overall is the dominant multiplicative loss in the derived SNR expression.

Our previous work experimentally measured the mixing efficiency of a DH system [10]. In this work, the mixing efficiency only depended on two efficiencies: the polarization efficiency and the spatial integration efficiency. Given rough surface scattering from a dielectric object, the depolarized signal interfered with a polarized reference, such that the polarization efficiency was 50%. Furthermore, the focal-plane array (FPA) used to digitally record the resulting hologram nominally had square pixels, which resulted in a sinc-like pixel modulation transfer function, such that the spatial integration efficiency was 74%. These two efficiencies described the measured mixing efficiency well at 37% because the signal was approximately path-length matched to the reference and did not limit the achievable SNR, since the coherence length of the MO laser was greater than 100 m.

In further experiments, we investigated the multiplicative losses due to coherence [11]. These experiments were significant because our results showed that the coherence efficiency, which is another efficiency that makes up the overall mixing efficiency, decreases quadratically with fringe visibility and that our measurements agreed well with our models. In particular, to degrade the temporal coherence of our MO laser, we used two approaches: sinusoidal phase modulation and linewidth broadening. The sinusoidal phase modulation produced spectral side bands and allowed us to simulate the effects of multiple-longitudinal modes in our MO laser. Phase modulation via pseudo-random bit sequences then allowed us to broaden the linewidth of our MO laser and simulate the effects of rapid fluctuations in the center frequency. Overall, our measurements agreed with our models to within 1.8% for sinusoidal phase modulation and 6.9% for linewidth broadening.

In both of these previous experiments [10], [11], we chose the FPA integration time based on the magnitude and stability

of the SNR to minimize environmental factors. As explored in this paper, these environmental factors can include laboratory vibrations and inherent hardware noise like laser flicker noise in the frequency of our MO laser. Accordingly, this paper experimentally demonstrates the impacts of laboratory vibrations and laser flicker noise on DH.

Vibrations in a DH system cause the interference fringes in the hologram to fluctuate across the FPA pixels. The source of the vibrations can be from a range of phenomena such as platform jitter, acoustic effects, etc. If the fringes fluctuate across the pixels over the course of the FPA integration time, then the vibrations smooth the detected fringes, reducing the fringe visibility, which is proportional to the mixing efficiency. If the FPA integration time is shorter than the rate of the fringe fluctuations, then the fringes are static over the FPA integration time and the multiplicative loss due to vibrations become negligible.

Since the MO laser spectrum and complex-degree of coherence are Fourier Transform pairs, the coherence length (and time) is inversely proportional to the laser linewidth. This relationship provides a gauge for the distance where the multiplicative loss due to coherence become significant. For larger-scale applications, a single-longitudinal-mode MO laser is necessary to achieve the narrow linewidths for acceptable performance at long ranges.

Note that previous efforts studied the noise sources contributing the laser linewidth [12]–[15]. One of the dominate noise sources can be laser flicker noise (also referred to as $1/f$ noise) [16], [17] and has a linewidth based on the observation time [18], [19]. Siegman first observed this phenomenon in 1967 [20] and a subsequent effort showed that it is due to the lifetimes of the charge carriers [21]. This outcome is of importance to us because when the laser linewidth becomes flicker-noise dominated, then the coherence efficiency becomes dependent on the FPA integration time (i.e., the observation time). Therefore, future efforts should also consider the laser frequency noise characteristics and the FPA integration time when assessing the performance of a DH system for large-scale applications.

In what follows, we specifically measure both the vibration efficiency and the coherence efficiency of our DH system. We do so at various FPA integration times and path-length differences between the signal and reference. Like in the previous experiments [10], [11], these efficiencies contribute to the overall mixing efficiency. New to this paper, however, is the fact that both the vibration efficiency and the coherence efficiency depend on the FPA integration time. In Section II, we first provide our mixing efficiency model that characterizes each performance-limiting effect as a multiplicative loss. Then in Section III we give the details on our experimental methodology to measure the mixing efficiency of our DH system. In Section IV, we then present the experimental results and analyze our model fits in relation to the mixing efficiency measurements. Last, we conclude this paper in Section V.

II. MIXING EFFICIENCY MODEL

Recall that the mixing efficiency, η_m, is a measure of how well the detected signal and reference interfere. Here, we define η_m, such that

$$\eta_m(\tau, t_i) = \eta_p \eta_s \eta_v(t_i) \eta_c(\tau, t_i), \tag{1}$$

where τ is the time delay between the signal and reference, t_i is the FPA integration time, η_p is the polarization efficiency, η_s is the spatial integration efficiency, η_v is the vibration efficiency, and η_c is the coherence efficiency. Also recall that we measured η_m, without the dependence on τ and t_i, in a previous experiment and found that $\eta_p = 50\%$ and $\eta_s = 74\%$ [10]. Since the experimental setup used in this paper is similar to that used in Ref. [10], we will use these values in the coming analysis.

The vibration efficiency, $\eta_v(t_i)$, in Eq. (1) captures the multiplicative loss in the achievable SNR from the blurring of the interference fringes in the hologram across the FPA pixels due to vibrations. If the FPA integration time t_i is faster than the vibrations, then $\eta_v(t_i) \approx 100\%$, and the fringes are stable over t_i. When vibrations occur during t_i, then $\eta_v(t_i) < 100\%$. We empirically determine this rule of thumb in the analysis that follows.

The coherence efficiency, $\eta_c(\tau, t_i)$, in Eq. (1) decreases quadratically with the fringe visibility, $\mathcal{V}(\tau, t_i)$, and also limits the achievable SNR. In practice, several coherence effects can degrade $\mathcal{V}(\tau, t_i)$, such as random power fluctuations, center frequency mismatch, and random phase fluctuations all between the signal and reference. Of the three phenomena, only the random power fluctuations and the random phase fluctuations depend on the FPA integration time, t_i, in addition to the time delay between the signal and reference, τ. However, the random power fluctuations would have to be significant for this phenomenon to be the dominate effect. This outcome is not the case in the ensuing experimental measurements. Therefore, we turn our attention to the random phase fluctuations, which we consider to be the dominate effect in the ensuing analysis [18].

To begin our model for the coherence efficiency, $\eta_c(\tau, t_i)$, we represent the complex-optical field, $U(t)$, of our MO laser as

$$U(t) = U_o \exp(j2\pi \overline{v} t) \exp[j\phi(t)], \tag{2}$$

where U_o is the amplitude, $\overline{v}$ is the mean center frequency, and $\phi(t)$ is the random phase fluctuations. In Eq. (2), we assume that the MO laser is a quasi-monochromatic light source with a constant amplitude and a linewidth due to $\phi(t)$. Next, we assume that $\phi(t)$ obeys a zero-mean Gaussian random process. Therefore, the random phase fluctuations of the signal light, $\phi_S(t_1)$, and the reference light, $\phi_R(t_2)$, also obey zero-mean Gaussian random processes, and so does the relative difference $\Delta\phi(t_1, t_2) = \phi_S(t_1) - \phi_R(t_2)$ [22]. We also assume that $\phi(t)$ is at least stationary in first increments, so that $\Delta\phi$ only depends on τ. As a result, $\langle\Delta\phi(\tau)\rangle = 0$ and the variance, $\sigma^2_{\Delta\phi}(\tau)$, follows as

$$\sigma^2_{\Delta\phi}(\tau) = \left\langle (\phi_S(t + \tau) - \phi_R(t))^2 \right\rangle. \tag{3}$$

Provided (3), we can relate the variance, $\sigma^2_{\Delta\phi}(\tau)$, to the complex degree of coherence, $\gamma(\tau)$. In practice, $\gamma(\tau)$ is a normalized correlation, and $\mathcal{V} = |\gamma(\tau)|$ when the amplitude

of the signal and reference are equal. We define $\gamma(\tau)$ in terms of the reference and signal as

$$\gamma(\tau) = \frac{\langle U_R^*(t)U_S(t+\tau)\rangle}{\langle U_R(0)U_S(0)\rangle},\qquad(4)$$

where U_R is the reference complex-optical field, U_S is the signal complex-optical field, and $\langle\cdot\rangle$ denotes an expectation operator [like in Eq. (3)]. Substituting Eq. (2) (with the appropriate subscripts) into Eq. (4) yields [23]

$$\gamma(\tau) = \langle\exp[j\Delta\phi(\tau)]\rangle = \exp\left[-\frac{1}{2}\sigma_{\Delta\phi}^2(\tau)\right].\qquad(5)$$

Note that in writing Eq. (5), we neglect any effects due to random amplitude fluctuations, but other works have considered these effects [18].

To further model $\sigma_{\Delta\phi}^2(\tau)$, we use the power spectral density (PSD) of the laser frequency noise, $\mathcal{G}_{\delta\nu}(f)$ [24]. In particular,

$$\sigma_{\Delta\phi}^2(\tau) = 4\pi^2\tau^2\int_0^\infty \mathcal{G}_{\delta\nu}(f)\,\mathrm{sinc}^2(f\tau)\,df,\qquad(6)$$

where $\mathrm{sinc}(0) = 1$ and $\mathrm{sinc}(x) = \sin(\pi x)/(\pi x)$ when $x \neq 0$. Note that the sinc^2 term in Eq. (6) acts as a low-pass filter on $\mathcal{G}_{\delta\nu}(f)$. Also note the in Eq. (6), $\sigma_{\Delta\phi}^2$ has two competing relationships with τ. First, $\sigma_{\Delta\phi}^2$ is quadractically proportional with τ, but $\sigma_{\Delta\phi}^2$ is also inversely proportional with τ because the cut-off frequency of the sinc^2 term decreases with increasing τ. This cut-off frequency ($\sim 1/\tau$) can be the approximate upper limit on $\mathcal{G}_{\delta\nu}$. However, $\sigma_{\Delta\phi}^2$ is still proportional to τ, since the quadratic relationship increases faster than the integral decreases, which makes physical sense. As τ increases, the signal and reference become more uncorrelated, and thus, $\sigma_{\Delta\phi}^2$ increases.

As an approximation, we model $\mathcal{G}_{\delta\nu}(f)$ in Eq. (6) as a linear combination of flicker and white noise [25], such that

$$\mathcal{G}_{\delta\nu}(f) = \frac{a}{f^\alpha} + \frac{\Delta\nu_o}{\pi},\qquad(7)$$

where a is the magnitude of the flicker noise, α is the log-power slope of the flicker noise ($1 \leq \alpha \leq 2$), and $\Delta\nu_o$ is the instantaneous linewidth due to white noise only. In the case when $\mathcal{G}_{\delta\nu}(f)$ is dominated by white noise, the MO laser PSD, $\mathcal{G}(\nu)$, has a Lorentzian lineshape and the integral in Eq. (6) converges. However, when $\mathcal{G}_{\delta\nu}(f)$ is dominated by flicker noise, $\mathcal{G}(\nu)$ has a Gaussian lineshape and Eq. (6) approaches infinity with a lower integration bound of zero. In reality, we have a finite measurement time, which acts as a high-pass filter and $f \lesssim 1/t_i$ is not captured by the measured $\sigma_{\Delta\phi}^2(\tau, t_i)$. Therefore, we add the high-pass filter to Eq. (6) [24] and the measured $\sigma_{\Delta\phi}^2$ becomes

$$\sigma_{\Delta\phi}^2(\tau, t_i) = 4\pi^2\tau^2\int_0^\infty \mathcal{G}_{\delta\nu}(f)\,\mathrm{sinc}^2(f\tau)$$
$$\times\left\{1 - \mathrm{sinc}^2[f(t_i-\tau)]\right\}df,\qquad(8)$$

so that the frequency range of interest for $\mathcal{G}_{\delta\nu}(f)$ is essentially $1/t_i$ to $1/\tau$. Note that all the approximations leading to and including Eq. (8) assumes $t_i > \tau$ and $t_i > \tau_c$.
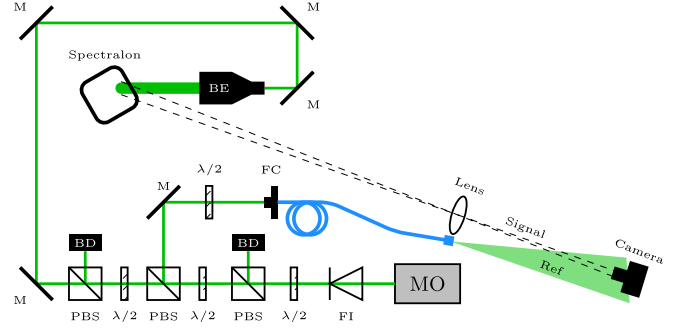

Fig. 1. An illustration of the experimental setup.

Since $\eta_c = |\gamma|^2$ [11], we substitute Eq. (8) into Eq. (5) and our model for η_c becomes

$$\eta_c(\tau, t_i) = \exp\left[-4\pi^2\tau^2\int_0^\infty \mathcal{G}_{\delta\nu}(f)\mathrm{sinc}^2(\pi f\tau)\right.$$
$$\left.\times\left\{1 - \mathrm{sinc}^2[f(t_i-\tau)]\right\}df\right].\qquad(9)$$

While this description is adequate, other models may be possible. Eq. (9) ultimately provides the closed-from expression needed to characterize the experimental results due to MO laser frequency noise in our DH system.

III. EXPERIMENTAL METHODS

This section details the experimental setup and data processing used to measure the mixing efficiency. The experimental setup and data processing is similar to that in Refs. [10] and [11], where additional details may be found.

A. Experiment Setup

Figure 1 shows the experimental setup. In the experiment, we used a cw, single-longitudinal-mode, Cobalt Samba diode-pumped solid-state laser with a wavelength of 532 nm as the MO laser. This laser provided 1W of power with a vendor specified linewidth <1 MHz and a coherence length $\ell_c > 100$ m. From previous work [11], we characterized the MO laser linewidth as $\Delta\nu < 500$ kHz, which corresponded to a minimum $\ell_c > 260$ m and a minimum $\tau_c > 875$ ns. We also used a Faraday isolator (FI) to prevent unwanted back reflection into the laser. To divert a portion of MO laser power, we used pairs of half-wave plates ($\lambda/2$) and polarizing beam splitters (PBS) to adjust the total power to a beam dump (BD) and to adjust the illuminator power to another BD. We used another pair of $\lambda/2$ and PBS to divert a portion of laser power for the local oscillator (LO), which we fiber coupled using another $\lambda/2$ to match the slow axis of the polarization maintaining (PM) fiber. We steered the illuminator using mirrors (M) and passed it through a beam expander (BE) to illuminate a sheet of Labsphere Spectralon which had a vendor specified 99% Lambertian reflectivity. Next, we imaged the scattered light onto the FPA associated with a Grasshopper3 camera, which is a 2048 × 1536 CMOS

array with a 3.45 μm square-pixel width, using a 1 in lens to create the signal. The distance from the Spectralon to the lens was 246 cm and the distance from the lens to the FPA was 41 cm. Here, the lens was a CVI Laser Optics' PLCX-C: laser grade plano convex spherical lens with a diameter of 1 in, focal length of 35 cm, and a 532 nm anti-reflective coating. To create the reference, we injected the fiber-coupled LO at the imaging lens and centered its diverging illumination onto the FPA to interfere with the converging signal.

With a 4 m LO fiber, we nearly matched the signal and reference path lengths to within a few centimeters. From our previous work, we experimentally determined the refractive index for the slow axis of the PM fiber to be ≈ 1.5 [11]. To vary the optical path length difference, $\Delta\ell$, we inserted a combination of 5 m, 10 m, 50 m, and 100 m length fiber for measurements at a $\Delta\ell = 0$ m, 7.5 m, 15 m, 22.5 m, 50 m, 72.5 m, 150 m, 172.5 m, 225 m, and 247.5 m, which corresponded to a maximum $\tau = 825$ ns. Additionally, we collected data at FPA integration times of $t_i = 100$ ms, 1 ms, and 100 μs. For comparison, t_i was greater than two to five orders of magnitude of the maximum τ and the suspected minimum τ_c.

For the collected data, we recorded full frames (i.e., 2048 $\times$ 1536 pixels) for a series of hologram, signal-only, and reference-only frames. We preformed speckle averaging by rotating the Spectralon between each speckle realization for a total of ten independent speckle realizations. We determined ten speckle realizations to be sufficient to reduce the speckle noise to about 5% [10]. For each speckle realization, we collected twenty holograms and twenty signal-only frames for shot-noise averaging. Additionally, we collected twenty reference frames-only frames between each speckle realization. In total, we collected 200 holograms, signal-only, and reference-only frames at each optical path length difference, $\Delta\ell$, and each FPA integration time, t_i.

B. Data Processing

We measured the mixing efficiency η_m at each $\Delta\ell$ and t_i. Note that we used full frames (i.e., 2048 $\times$ 1536 pixels) for the data processing. To measure η_m, we used the 2D-Fast Fourier Transform of each hologram and windowed the pupil in the Fourier plane. This windowed pupil also contained noise, so we reflected the pupil window along the y-axis in the Fourier plane and estimated the noise in the adjacent quadrant of the Fourier plane. Note that by measuring the noise this way, we assumed the noise is symmetric in the Fourier plane over the window. Then, we subtracted the estimated noise from the measured windowed pupil. The average over the Fourier plane windowed pupil without noise and over all frames was the average heterodyne energy $\overline{E}_H$. The average over all frames for the signal-only and reference-only frames was $\overline{m}_S$ and $\overline{m}_R$, respectively. Lastly, we measured the mixing efficiency, η'_m, using the following formula:

$$\eta'_m = \frac{\pi}{4q_I^2} \frac{\langle \overline{E}_H(x,y) \rangle}{\langle \overline{m}_S(x,y) \overline{m}_R(x,y) \rangle}, \tag{10}$$

where here, $\langle \cdot \rangle$ is the spatial average over all pixels and q_I is the image plane sampling quotient, which we measured to
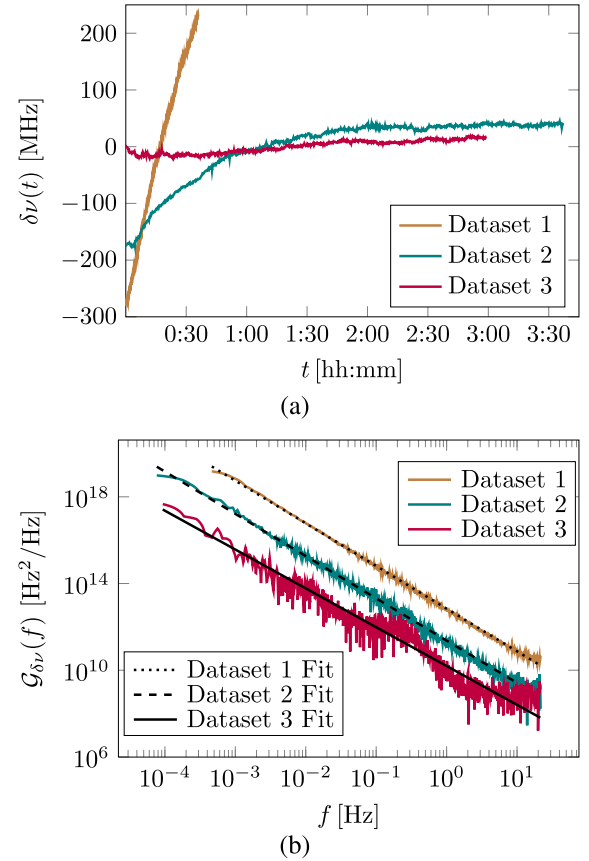

Fig. 2. (a) MO laser center frequency measurements for the three datasets. (b) The power spectral density of each data set from (a) with a fit of Eq. (11).

be 2.7 [26]. The $\pi/4 \, q_I^2$ term in Eq. 10 is the ratio of the total number of pixels to the number of pixels in the Fourier plane pupil window, since $\overline{E}_H$ is averaged over less pixels than $\overline{m}_S$ and $\overline{m}_R$.

C. Measured MO Laser Frequency Noise

We measured the MO laser's center frequency over time with a HighFinesse WU-2 wavemeter, which has a measurement resolution of ≈ 2 MHz and samples at ≈ 20 Hz. We took three datasets during the course of a day: dataset 1, which was minutes after the laser was locked onto single-frequency operation; dataset 2, which was an hour after the completion of dataset 1; and dataset 3, which was minutes after the completion of dataset 2. Figure 2(a) shows these laser frequency measurements, where we subtracted the mean from each respective dataset to represent the frequency fluctuations $\delta\nu$. In dataset 1 of Fig. 2(a), we observed the center frequency rise on the order of 240 Hz/s for 30 minutes. Even though a difference in center frequency between the signal and reference would decrease the coherence efficiency, and the loss would increase over the optical path length difference, $\Delta\ell$, the maximum frequency difference over the maximum $\Delta\ell$ was less than 1 Hz. Therefore, this center frequency difference was negligible.
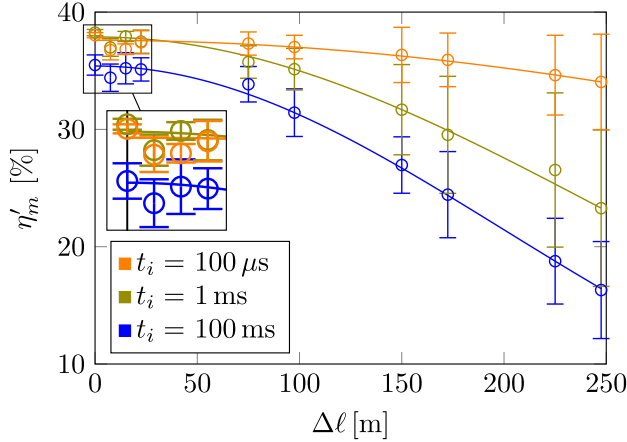
To further analyze the data, we calculated the PSD of the frequency noise, $G_{\delta\nu}$, for each data set as shown in Fig. 2(b). We observed flicker noise in each dataset of $G_{\delta\nu}$. To quantify

TABLE I

FLICKER NOISE FIT COEFFICIENTS

Dataset	1	2	3
a	12.8	11.3	10.2
α	1.98	1.96	1.79

TABLE II

GAUSSIAN FIT COEFFICIENTS

t_i	100 ms	1 ms	100 μs
A [%]	35	37	37
$\Delta\nu$ [kHz]	400	320	140

Fig. 3. The mixing efficiency measurements η'_m (○) with error bars $\pm\sigma$ and a Gaussian fit (−) to the data.

this flicker noise, we used the first term of Eq. (7) (i.e., the flicker noise term) and modified the amplitude coefficient for a fit with the following equation:

$$\mathcal{G}_{\delta\nu}(f) = 10^a/f^{-\alpha}, \qquad (11)$$

where a and α were the fit coefficients. The fit results of Eq. (11) are shown in Table I, where the fit coefficients were rounded one digit up from the fit uncertainty (e.g. $1.06 \pm 0.01 = 1.1$). We observed that the magnitude and slope of the flicker noise was slightly different between datasets, which shows that the flicker noise was not constant throughout the day. Note that each η'_m dataset for a single t_i took about a day to record at each $\Delta\ell$, so the three wavemeter datasets here were examples of the flicker noise strength in the upcoming η'_m results (cf. Fig. 3). Additionally, the sampling frequency of the wavemeter ($\sim 20\,\mathrm{Hz}$) was insignificant to obtain a $\mathcal{G}_{\delta\nu}$ useful for our range of measurements ($1/t_i - 1/\tau = 10\ Hz - GHz$). However, these wavemeter results show that our MO laser frequency noise was flicker-noise dominated from 0.1 mHz - 20 Hz. We will use these findings in the ensuing analysis of our experimental results for η'_m.

IV. EXPERIMENTAL RESULTS AND ANALYSIS

In this section, we analyze our experimental results in two steps. For the first step, we show the measured mixing efficiency, η'_m, results to analyze the vibration efficiency, η_v, and the coherence efficiency, η_c. Then, for the second step, we measured the coherence efficiency from η'_m, which provided the measured coherence efficiency, η'_c, to compare to our model using Eq. (9).

A. Mixing Efficiency, η'_m

Figure 3 shows the η'_m results with the error bars $\pm$ the standard deviation of the measurement, $\sigma_{\eta'_m}$. Because we assumed η_v was only dependent on t_i, we assumed that the change in $\eta'_m(\Delta\ell)$ was only dependent on η_c. As a reminder from our model in Eq. 1 and 9, we assumed η_c is only dependent on $\Delta\ell$ (i.e., $\Delta\ell = c\tau$). Therefore, we fit each t_i dataset to the following Gaussian function

$$\eta_m(\Delta\ell) = A \exp\left[-\left(\frac{\pi\,\Delta\nu\,\Delta\ell}{\sqrt{2\log(2)}c}\right)^2\right], \qquad (12)$$

where $\Delta\nu$ is the observed laser linewidth and A is the relative amplitude. The mean percent difference (i.e., $100 \times |\eta_m - \eta'_m|/\eta_m$) was 0.9%. Eq. (12) represents the magnitude-squared of Eq. (5) [i.e., $|\gamma(\tau)|^2$] for a Gaussian lineshape of the MO laser PSD, $\mathcal{G}(\nu)$, such that $\mathcal{G}_{\delta\nu}(\nu)$ in Eq. (6) is flicker noise dominated. We chose to fit a Gaussian function because the fit results were much better than fitting to a decaying exponential function, where the mean percent difference was 3.7%. Note that a decaying exponential function corresponds to a Lorentzian lineshape for $\mathcal{G}(\nu)$, such that $\mathcal{G}_{\delta\nu}(\nu)$ would then be white noise dominated [cf. Eq. (7)]. This outcome indicates that our MO laser was flicker noise dominated, as seen in the wavemeter measurements (cf. Section III-C).

Table II shows the Eq. (12) fit results, where we rounded to the next digit up from the fit coefficient uncertainty. First, we observed that A increased 2.5% from $t_i = 100\,\mathrm{ms}$ to 1 ms and 100 μs. Even though our DH system was on an active pneumatic isolated optical table and we eliminated all vibrational sources within our control, we believe this increase was due to residual vibrations from laboratory pumps on the ground and acoustic vibrations from the laboratory pumps, the air handlers, etc. We observed that the vibrations were negligible at $t_i = 1\,\mathrm{ms}$ since the A's are approximately the same for $t_i = 1\,\mathrm{ms}$ and 100 μs. Therefore, we estimated $\eta'_v = 94\%$ for $t_i = 100\,\mathrm{ms}$ and $\eta'_v = 100\%$ for $t_i = 1\,\mathrm{ms}$ and 100 μs. Note that the value of 37% for $t_i = 1\,\mathrm{ms}$ and 100 μs agrees with our previous measurements [10]. In addition, we observed $\Delta\nu$ decreased by 65% when t_i decreased from 100 ms to 100 μs. This outcome corresponded to τ_c increasing from 1.7 μs to 4.6 μs and ℓ_c increasing from 500 m to 1.4 km, which is a 280% increase. Note that later representations of this data will be divided by the fit coefficient A to represent η'_c.

We noticed a few additional features in Fig. 3. First, the dip in the datasets at 7.5 m was apparent in all three datasets. This feature illustrated that the laser PSD was not a smooth, symmetric Gaussian [27] and was probably not experimental error. Secondly, we observed that $\sigma_{\eta'_m}$ increased as
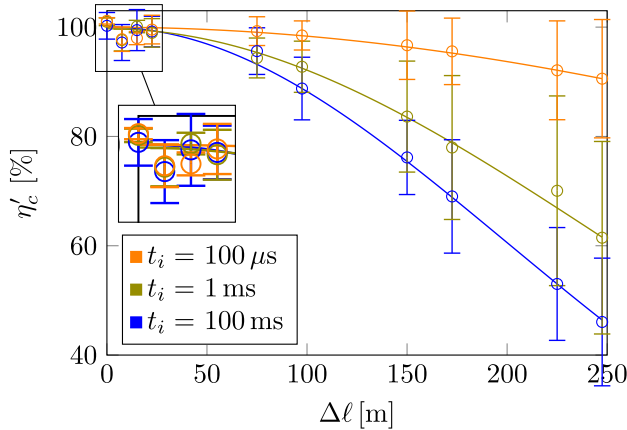
Fig. 4. η_c' results (○) with error bars $\pm\sigma$ and an independent fit for each t_i using Eq. (9) (—).

TABLE III

FREQUENCY NOISE FIT COEFFICIENTS

t_i	100 ms	1 ms	100 μs
a	10.9	12.5	12.5
$\Delta\nu_o$ [kHz]	0.00	0.00	0.00

$\Delta\ell$ increased. We expected this outcome because $\Delta\phi$ fluctuates more as $\Delta\ell$ increases, and the measurements became noisier. Lastly, we observed a few data points deviated slightly more from the Gaussian fit than others. We believe this behavior was because the laser frequency noise varied slightly over the course of all measurements, as seen in the three different wavemeter measurements (cf. Section III-C).

B. Coherence Efficiency, η_c'

The purpose of estimating η_c' was to compare our measurements to our η_c model [cf. Eq. (9)] and to see what additional information can be gleaned. Recall that our wavemeter measurements (cf. Sec III-C) and the η_m' fit to Gaussian function indicates that our MO laser frequency noise was flicker noise dominated instead of white noise dominated. However, if we were approaching the white noise limit (i.e., $\mathcal{G}_{\delta\nu}(f)$ was neither flicker nor white noise dominated), then η_c' would be a multiplicative combination of a Gaussian and decaying exponential, which yields by the Voigt lineshape for $\mathcal{G}(\nu)$ [25]. Therefore, by using Eq. (9) to include both flicker and white noise in $\mathcal{G}_{\delta\nu}(f)$ [cf. Eq. (7)], then the fits to η_c' will provide additional information.

We estimated η_c' by dividing η_m' by A from Table II, which effectively removes all other efficiencies associated with η_m from our model [cf. Eq. (1)]. Note that the difference between η_m' and η_c' is the y-intercept and not the shape. In Figure 4, we show η_c' with a fit of Eq. (9), where the mean percent difference was 0.9%, the same as Sec. IV-A. We chose a and $\Delta\nu_o$ to be the fit coefficients and $\alpha = 1.91$, which is the mean from Table I, for $\mathcal{G}_{\delta\nu}(f)$. Note that we fixed the value for α because the fits were over determined when α was a fit coefficient and the coefficient uncertainties were unreasonable. Table III shows the fit coefficient results, where we rounded to the next digit up from the fit coefficient uncertainty.

From our fit results, $\Delta\nu_o$ was minimized to zero, which strongly indicates that our measurements were not approaching the white noise limit. One point to consider was that our maximum $\Delta\ell = 245$ m limited the range of η_c' and possibly limited our ability to estimate the white noise limit. However, the η_c difference between the white noise (i.e., a decaying

exponential) and the flicker noise (i.e., a Gaussian) is most apparent at shorter $\Delta\ell$ (i.e., closer to zero). To further examine our ability to estimate the white noise with our data, we forced the fits to include a $\Delta\nu_o = 10$ kHz. This addition of white noise increased the mean percent difference to 1.1% and the mean percent error increased more as we increased $\Delta\nu_o$ above 10 kHz. This outcome showed that our model [cf. Eq. (9)] should be sensitive enough when the white noise is on the order for the flicker noise. Therefore, we safely assumed that none of the measurements approached the white noise floor within an order of magnitude of the flicker noise of the MO laser and a further reduction in t_i would further decrease our observed linewidth and increase the τ_c and ℓ_c.

V. CONCLUSION

In this paper, we presented a complete model for the mixing efficiency of a DH system to account for vibrational and laser frequency noise effects. Our mixing efficiency model contained four independent efficiencies from different phenomenon: polarization (50%), spatial-fringe integration (74%), vibrations, and coherence. We experimentally measured the mixing efficiency at various optical path differences between the signal and reference, and at different integration times. At zero path length difference between the signal and reference, we observed the mixing efficiency decreased for the longest integration time, which we attributed to vibrations (94%). When the integration time was ≤ 1 ms, then the vibration efficiency was maximized (100%).

The measured mixing efficiency had a Gaussian shape with respect to the path length difference and the observed linewidth decreased by 65% when we decreased the integration time from 100 ms to 100 μs. This outcome correlated to increasing the effective coherence length by 280%. These results indicated that the MO laser frequency noise was dominated by flicker noise. We developed a model for the coherence efficiency, which incorporates the effects of the laser frequency noise and fit the model to the estimated coherence efficiency from the mixing efficiency measurements. The results confirmed that the MO laser frequency noise was flicker noise dominated, not approaching the white noise limit, and that a further reduction in the integration time would increase coherence efficiency over range (i.e., increase the effective coherence length).

Overall, we showed that the hologram integration time should be considered in the design of a DH system. Decreasing the integration time reduces vibration losses and increases the effective coherence length of the MO laser when the MO frequency noise is dominated by flicker noise. These hologram integration time effects present a trade space with respect to the vibration efficiency, coherence efficiency, and signal strength for the performance of a DH system.

References

[1] G. Pedrini and H. J. Tiziani, "Short-coherence digital microscopy by use of a lensless holographic imaging system," *Appl. Opt.*, vol. 41, no. 22, pp. 4489–4496, 2002.

[2] I. Yamaguchi, "Phase-shifting digital holography," in *Optics Photonics News*. Washington, DC, USA: OSA, Jul. 2008, pp. 48–53.

[3] W. Osten *et al.*, "Recent advances in digital holography [Invited]," *Appl. Opt.*, vol. 53, no. 27, pp. G44–G63, 2014. [Online]. Available: http://ao.osa.org/abstract.cfm?URI=ao-53-27-G44

[4] M. F. Spencer, R. A. Raynor, M. T. Banet, and D. K. Marker, "Deep-turbulence wavefront sensing using digital-holographic detection in the off-axis image plane recording geometry," *Opt. Eng.*, vol. 56, no. 3, 2016, Art. no. 031213.

[5] M. T. Banet, M. F. Spencer, and R. A. Raynor, "Digital-holographic detection in the off-axis pupil plane recording geometry for deep-turbulence wavefront sensing," *Appl. Opt.*, vol. 57, no. 3, pp. 465–475, 2018.

[6] D. E. Thornton, M. F. Spencer, and G. P. Perram, "Deep-turbulence wavefront sensing using digital holography in the on-axis phase shifting recording geometry with comparisons to the self-referencing interferometer," *Appl. Opt.*, vol. 58, no. 5, pp. A179–A189, 2019.

[7] C. J. Pellizzari, M. F. Spencer, and C. A. Bouman, "Phase-error estimation and image reconstruction from digital-holography data using a Bayesian framework," *J. Opt. Soc. Amer. A, Opt. Image Sci.*, vol. 34, no. 9, pp. 1659–1669, 2017.

[8] C. J. Pellizzari, M. T. Banet, M. F. Spencer, and C. A. Bouman, "Demonstration of single-shot digital holography using a Bayesian framework," *J. Opt. Soc. Amer. A, Opt. Image Sci.*, vol. 35, no. 1, pp. 103–107, 2018.

[9] C. J. Pellizzari, M. F. Spencer, and C. A. Bouman, "Imaging through distributed-volume aberrations using single-shot digital holography," *J. Opt. Soc. Amer. A, Opt. Image Sci.*, vol. 36, no. 2, pp. A20–A33, 2019.

[10] D. E. Thornton, M. F. Spencer, C. A. Rice, and G. P. Perram, "Digital holography efficiency measurements with excess noise," *Appl. Opt.*, vol. 58, no. 34, pp. G19–G30, 2019.

[11] D. E. Thornton, D. Mao, M. F. Spencer, C. A. Rice, and G. P. Perram, "Digital holography experiments with degraded temporal coherence," *Opt. Eng.*, vol. 59, no. 10, 2020, Art. no. 102406.

[12] S. Piazzolla, P. Spano, and M. Tamburrini, "Characterization of phase noise in semiconductor lasers," *Appl. Phys. Lett.*, vol. 41, no. 695, pp. 1981–1983, 1982.

[13] B. Daino, P. Spano, M. Tamburrini, and S. Piazzolla, "Phase noise and spectral line shape in semiconductor lasers," *IEEE J. Quantum Electron.*, vol. 19, no. 3, pp. 266–270, Mar. 1983.

[14] C. Henry, "Theory of the phase noise and power spectrum of a single mode injection laser," *IEEE J. Quantum Electron.*, vol. 19, no. 9, pp. 1391–1397, Sep. 1983.

[15] M. Osinski and J. Buus, "Linewidth broadening factor in semiconductor lasers–An overview," *IEEE J. Quantum Electron.*, vol. 23, no. 1, pp. 9–29, Jan. 1987.

[16] L. B. Mercer, "1/f frequency noise effects on self-heterodyne linewidth measurements," *J. Lightw. Technol.*, vol. 9, no. 4, pp. 485–493, Apr. 1991.

[17] Y. Salvadé and R. Dändliker, "Limitations of interferometry due to the flicker noise of laser diodes," *J. Opt. Soc. Amer. A, Opt. Image Sci.*, vol. 17, no. 5, pp. 927–932, 2000.

[18] K. Petermann, *Laser Diode Modulation and Noise*. Norwell, MA, USA: Kluwer, 1988.

[19] G. Di Domenico, S. Schilt, and P. Thomann, "Simple approach to the relation between laser frequency noise and laser line shape," *Appl. Opt.*, vol. 49, no. 25, pp. 4801–4807, 2010.

[20] A. Siegman, B. Daino, and K. Manes, "Preliminary measurements of laser short-term frequency fluctuations," *IEEE J. Quantum Electron.*, vol. 3, no. 5, pp. 180–189, May 1967.

[21] A. van der Ziel, "Noise in solid-state devices and lasers," *Proc. IEEE*, vol. 58, no. 8, pp. 1178–1206, Aug. 1970.

[22] J. W. Goodman, *Statistical Optics*, 2nd ed. Hoboken, NJ, USA: Wiley, 2015.

[23] A. Papoulis, *Probability, Random Variables, and Stochastic Processes*, 3rd ed. New York, NY, USA: McGraw-Hill, 1991.

[24] L. S. Cutler and C. L. Searle, "Some aspects of the theory and measurement of frequency fluctuations in frequency standards," *Proc. IEEE*, vol. 54, no. 2, pp. 136–154, Feb. 1966.

[25] G. M. Stéphan, T. T. Tam, S. Blin, P. Besnard, and M. Têtu, "Laser line shape and spectral density of frequency noise," *Phys. Rev. A, Gen. Phys.*, vol. 71, no. 4, pp. 1–9, Apr. 2005.

[26] M. F. Spencer, "Spatial heterodyne," in *Encyclopedia of Modern Optics II*, vol. 4. Amsterdam, The Netherlands: Elsevier, 2017, pp. 369–400.

[27] J. T. Verdeyen, *Laser Electron.*, 3rd ed. Upper Saddle River, NJ, USA: Prentice-Hall, 1995.

Douglas E. Thornton received the B.S. degree in electrical engineering from the Rose-Hulman Institute of Technology in 2008, the M.S. degree in electrical engineering from the Air Force Institute of Technology (AFIT) with a focus on electro-optics and laser spectroscopy in 2010, and the Ph.D. degree in applied physics from AFIT in 2019. After graduation, he commissioned in the U.S. Air Force as a Developmental Engineer and Attended at AFIT. He is an Active Member in SPIE, OSA, and IEEE professional societies, along with Tau Beta Pi and Eta Kappa Nu honor societies.

Mark F. Spencer received the B.S. degree in physics from the University of Redlands in 2008 and the M.S. and Ph.D. degrees in optical sciences and engineering from AFIT in 2011 and 2014, respectively. He is currently a Senior Research Physicist and the Principal Investigator for the Aero Effects and Beam Control Program with Air Force Research Laboratory within the Directed Energy Directorate. He is also an Adjunct Assistant Professor of optical sciences and engineering with the Department of Engineering Physics, Air Force Institute of Technology. In addition to being a Senior Member of SPIE, he is a regular member of OSA and DEPS.

Christopher A. Rice received the B.S. degree in electrical engineering from Cedarville University, the M.S. degree in electrical engineering and the Ph.D. degree in optical sciences and engineering from AFIT. He currently serves as a Research Assistant Professor with the Department of Engineering Physics, Air Force Institute of Technology (AFIT). He is interested in topic areas related to high-energy lasers, remote sensing, laser lethality, and optical diagnostics. His work on specific research topics currently include atmospheric propagation of high energy lasers, diode pumped alkali and rare gas laser gain cell construction, novel laser demonstration, aerosol field measurements, modeling, simulation, and validation of directed energy simulations, pulsed laser ablation of titanium and carbon, and new techniques of turbulence characterization over open paths.

Glen P. Perram received the B.S. degree in applied and engineering physics from Cornell University in 1980 and the Ph.D. degree in physics from AFIT in 1986. He has been a Professor of physics with the Air Force Institute of Technology since 1989. He is a fellow of the Directed Energy Professional Society. He is a registered professional engineer at the State of Ohio. He received the 2013 Air Force Outstanding Civilian Senior Scientist Award for his work on Diode Pumped Alkali Lasers and the General Bernard A. Schriever Award for advancing aerospace power in 1995.